

DETERMINATION OF THE PRIMORDIAL HELIUM ABUNDANCE BASED ON NGC 346 AN H II REGION OF THE SMALL MAGELLANIC CLOUD

MABEL VALERDI, ANTONIO PEIMBERT, MANUEL PEIMBERT, & ANDRÉS SIXTOS

Instituto de Astronomía, Universidad Nacional Autónoma de México, Apdo. Postal 70-264 Ciudad Universitaria, México

Draft version April 4, 2019

ABSTRACT

To place meaningful constraints on Big Bang Nucleosynthesis models, the primordial helium abundance determination is crucial. Low-metallicity H II regions have been used to estimate it since their statistical uncertainties are relatively small. We present a new determination of the primordial helium abundance, based on long slit spectra of the H II region NGC 346 in the small Magellanic cloud. We obtained spectra using three $409'' \times 0.51''$ slits divided in 97 subsets. They cover the range $\lambda\lambda 3600-7400$ of the electromagnetic spectrum. We used P_YNeB and standard reduction procedures to determine the physical conditions and chemical composition. We found that for NGC 346: $X = 0.7465$, $Y = 0.2505$ and $Z = 0.0030$. By assuming $\Delta Y/\Delta O = 3.3 \pm 0.7$ we found that the primordial helium abundance is $Y_p = 0.2451 \pm 0.0026$ (1σ). Our Y_p value is in agreement with the value of neutrino families, N_ν , and with the neutron half-life time, τ_n , obtained in the laboratory.

Keywords: ISM: abundances — galaxies: ISM — primordial nucleosynthesis — H II regions — Magellanic Clouds

1. INTRODUCTION

A highly accurate ($\lesssim 1\%$) primordial helium abundance (Y_p) determination plays an important role in understanding the Universe. In particular, it is extremely important to constrain: Big Bang Nucleosynthesis models, elementary particle physics and the study of galactic chemical evolution.

To obtain a value for Y_p using H II regions, it is necessary to use the relation between the helium mass fraction (Y) and the heavy elements mass fraction (Z). The relation is then extrapolated to zero metallicity to estimate the primordial mass fraction of helium. The first determination of Y_p based on observations of H II regions was carried out by Peimbert & Torres-Peimbert (1974). Since then, many estimations have been done using this technique (e.g., Izotov et al. 2014; Aver et al. 2015). This method has been modified to use the O abundance instead of Z , because measuring other chemical elements becomes impractical. Although some groups seek alternatives to O, like using N or S (e.g. Pagel et al. 1992; Fernández et al. 2018).

In recent years, careful studies with high quality determinations of Y_p have been done by: Izotov et al. (2014), Aver et al. (2015), Peimbert et al. (2016), and Fernández et al. (2018). To diminish the uncertainties most determinations use many objects; but large samples only diminish the contribution of statistical errors, while systematic errors are not diminished; in fact, if one is not careful, systematic errors can be more significant for large samples, since low quality objects/observations are often included (e.g., Peimbert et al. 2000, 2007; Ferland et al. 2010).

Low-metallicity H II regions have permitted to estimate the primordial helium abundance, whose statistical uncertainties are very small ($\lesssim 1\%$) (e.g. Izotov et al. 2014); nevertheless, due to the numerous systematic uncertainties, obtaining better than 1% precision for individual objects remains a challenge.

The Small Magellanic Cloud (SMC) hosts the region NGC 346, this is the best H II region to determine Y_p . This is the brightest and largest H II region of the SMC. Its $H\alpha$ intensity places it on the boundary between normal and giant

extragalactic H II regions. In addition, its proximity, at a distance of 61 ± 1 Kpc (Hilditch et al. 2005), makes it possible to resolve individual stars and to avoid their contributions to the observed nebular spectra. We also note that NGC 346 hosts the largest sample of O-type stars in the entire SMC (Massey et al. 1989).

NGC 346 possesses some definite advantages over other H II regions: as it is a nearby object, the underlying absorption correction (due to the stellar absorption of the H and He lines) can be reduced significantly, at least by an order of magnitude; another advantage of its proximity is that it can be observed in different lines of sight, this has been used to rule out the presence of a significant helium ionization correction factor (ICF; e.g. Vilchez 1989; Mathis & Rosa 1991; Peimbert et al. 1992; Viegas et al. 2000; Zhang & Liu 2003); another important characteristic is that the electronic temperature is smaller than in the less metallic H II regions, this reduces the effect of collisional excitation of the ground level of H^0 ; its metallicity ($Z \sim 0.003$; $\sim 20\%$ of solar) requires a small extrapolation to derive Y_p . However, it has the disadvantage that the correction for its chemical evolution, is larger than in many other objects used for the determination of Y_p (Peimbert et al. 2000). Overall there is no H II region that is simultaneously at least as close, as large, and with a metallicity as low as NGC 346.

In this paper, we present a very precise primordial helium abundance determination. For this we use a single H II region, NGC 346, which is probably the best object for this determination, for the reasons mentioned before, see the comment by Steigman in Ferland et al. (2010). Additionally, we include a detailed study of the sources of error involved in this determination, along with a justification of using a single H II region to determine Y_p .

The paper is organized as follows: Section 2 presents the characteristics of the observations and the data reduction. The line intensity corrections due to extinction and underlying absorption are presented in Section 3. Section 4 shows the determination of physical conditions, using both recombination lines (RLs) and collisional excitation lines (CELs). Sections 5 and 6 show the determination of chemical abundances, the determination of ionic abundances and of total abundances re-

spectively. Finally, the determination of the primordial helium abundance, and the conclusions are shown in sections 7 and 8.

2. SPECTROSCOPIC OBSERVATIONS

We obtained long-slit spectra with the Focal Reducer Low Dispersion Spectrograph FORS1, the night of 2002 September 10 at the Very Large Telescope Facility (VLT), located at Melipal, Chile for the H II region NGC 346 ($\alpha = 00^h59^m05^s.0$ $\delta = -72^\circ10'38''$). We used three grism configurations: GRIS-600B+12, GRIS-600R+14 with the filter GG435, and GRIS-300V with the filter GG375.

Table 1
Observation Settings.

Grism	Filter	λ (Å)	Resolution ($\lambda/\Delta\lambda$)	Exp. time (s)
600B+12	–	3560 - 5974	1300	720 × 3
600R+14	GG435	5330 - 7485	1700	600 × 3
300V	GG375	3440 - 7600	700	120 × 3

Table 1 shows the resolution and wavelength coverage for the emission lines observed with each grism. We chose this resolution as a compromise: seeking high resolution without breaking the spectra into too many segments.

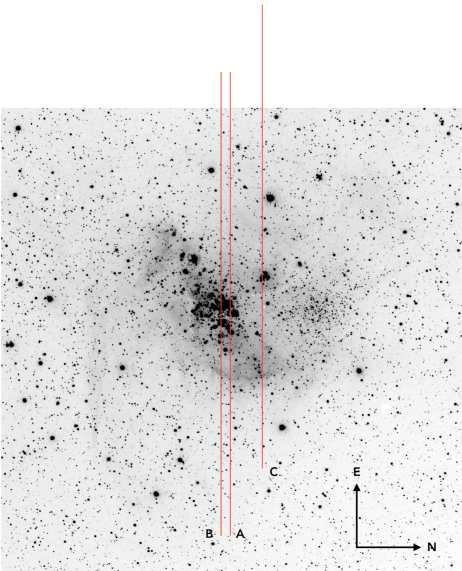


Figure 1. VLT images of NGC 346 in the SMC. This object is located at $\alpha = 00^h59^m05^s.0$, $\delta = -72^\circ10'38''$.

The slit width and length were $0''.51$ and $410''$ respectively. We have three different positions of the slit in the nebula: from the first position A (slit position $\alpha = 00^h59^m06^s$ $\delta = -72^\circ10'29.3''$), we defined 32 extraction windows; from the second position B (slit position $\alpha = 00^h59^m06^s$ $\delta = -72^\circ10'37.3''$), we defined 31 extraction windows; and from the last position C (slit position $\alpha = 00^h59^m19^s$ $\delta = -72^\circ10'0.7''$), we defined 34 extraction windows. The limits for each window were selected to avoid regions with qualitatively different spectra (e.g. stars or clouds) or to break long

regions into more homogeneous bits. To keep the same observed region within the slit, we used the LACD (linear atmospheric dispersion corrector) regardless of the air mass value.

We used IRAF to reduce the spectra, following the standard procedure; bias, dark and flat correction, wavelength calibration, flux calibration, spectra extraction. We use the low-resolution data to tie the calibration of the blue and red spectra by calibrating the brightest (blue and red) lines to the low-resolution spectra. For the flux calibration we used the standard stars LTT 2415, LTT 7389, LTT 7987, and EG 21 by Hamuy et al. (1992, 1994). We did an analysis of the full sample, for each spectrum, in the three slit positions A, B, and C.

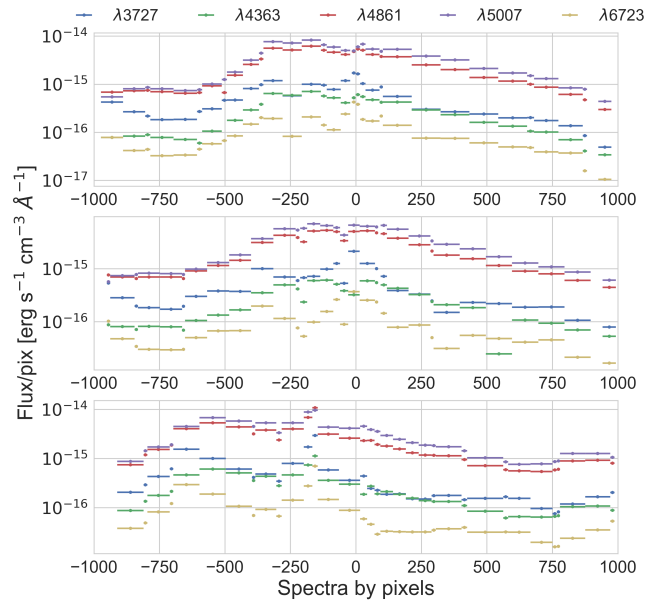


Figure 2. The plot shows the intensity of the five emission lines ($\lambda 3727$, $\lambda 4363$, $\lambda 4861$, $\lambda 5007$, and $\lambda 6717 + 31$) in the 97 windows for each slit A, B and C (up, middle and down respectively). On the x axis, the bar corresponds to the number of pixels that each window contains. The slits are centered in pixel zero.

We did a rough analysis of each of our 97 windows; in it we measured $H\beta$ (as a measure of the overall intensity), $[O II] \lambda 3727$ (as a measure of O^+), $[O III] \lambda 5007$ (as a measure of O^{++}), $[O III] \lambda 4363$ (as a measure of the quality of the temperature), and $[S II] \lambda 6717 + 31$ (as a measure of the quality of the density); see Figure 2. We also present the equivalent width of $H\beta$ in emission (to estimate the influence of the underlying absorption); see Figure 3. In a future paper, we will present the line intensities for each of the 97 windows.

We want to select the windows that cover the brightest parts while avoiding regions where there is too much stellar continuum (i.e. we remove the brightest stars to avoid the effect of stellar underlying absorption, see Figure 1).

To minimize the errors of the emission lines we define a new region, Region I, summing the windows with best data. We selected which windows to include in Region I using 3 criteria: they needed to be bright, to have a high equivalent width in emission, and latter we will see that there was some Wolf-Rayet He II emission that we tried to diminish. We find that windows with a high equivalent width in emission are brighter than $I(H\beta) = 2 \times 10^{-15} \text{ erg s}^{-1} \text{ cm}^{-3} \text{ \AA}^{-1}$ per pixel.

Finally, we are left with regions that have $EW(H\beta) > 150$, and that do not show Wolf-Rayet contamination in He II $\lambda 4686$. Region I was lastly composed of 20 windows (A10, A12, A13, A14, A21, A23, A24, B10, B11, B14, B22, B23, C3, C5, C6, C7, C9, C11, C14, and C15). In Figures 4, and 5, we show the blue and red spectra of Region I.

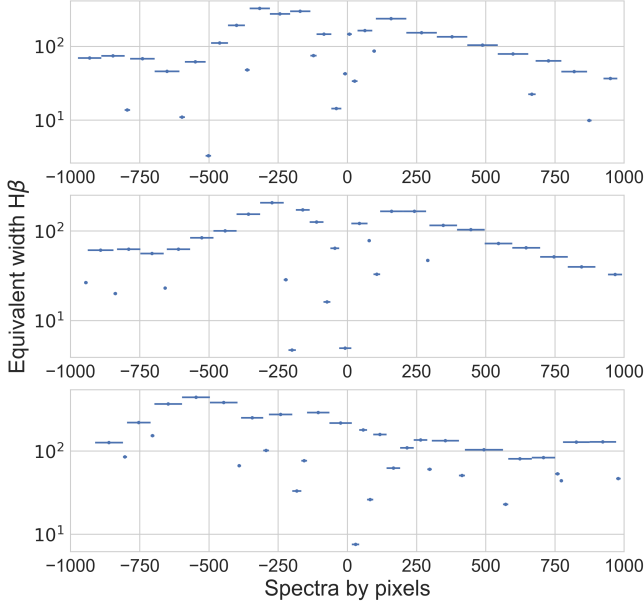


Figure 3. The plot shows the $EW(H\beta)$ for each window in three slit positions. Section A, B and C (up, middle and down respectively). On the x axis, the bar corresponds to the number of pixels that each window contains. The slits are centered in pixel zero.

3. LINE INTENSITIES AND REDDENING CORRECTION

Emission line flux measurements were made with the `SPLIT` routine of the `IRAF` package. These were measured by integrating all the flux in the line between two given limits and by subtracting the local continuum estimated by eye. Partially blended lines were deblended with two or three Gaussian profiles to measure the individual line fluxes and we forced the lines to have the same widths.

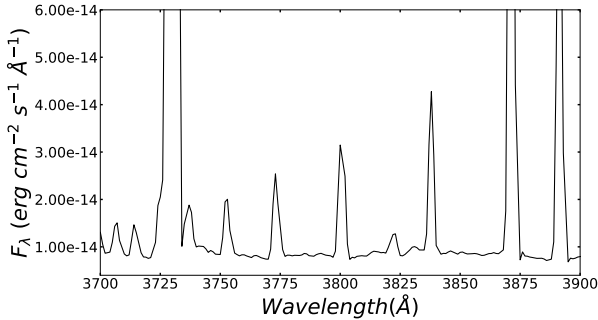


Figure 4. Plot of a fraction of the observed wavelength blue range for the high-resolution spectrum of the chosen extractions.

We derived the reddening by fitting the observed flux ratios of the brightest Balmer lines to the theoretical values normalized to the $H\beta$ flux. We estimated the theoretical Balmer

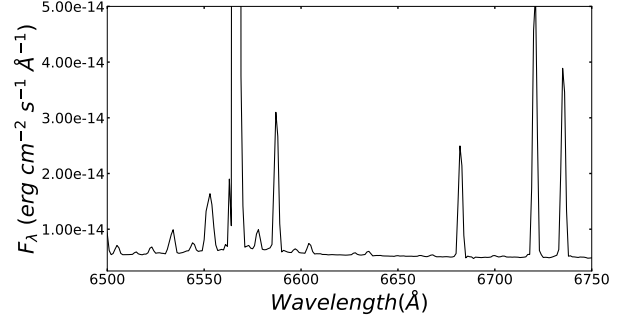


Figure 5. Plot of a fraction of the observed wavelength red range for high-resolution spectrum of the chosen extractions.

decrement using the data by Storey & Hummer (1995) assuming $T_e = 12500$ K, and $n_e = 100 \text{ cm}^{-3}$. We used the extinction law of Seaton (1979). We assumed that the underlying absorption had the form $EW_{abs}(Hn) = EW_{abs}(H\beta) \times g(Hn)$, where $g(Hn)$ was obtained from Table 2 of Peña-Guerrero et al. (2012). We produced a stellar template normalized to $EW_{abs}(H\beta)$ based in the low metallicity instantaneous burst models from González Delgado et al. (1999), to correct for the underlying absorption equivalent widths (EW s) for the Balmer lines. The percent error for each line includes the uncertainties in the reddening correction and the uncertainties in underlying absorption.

The underlying absorption, reddening correction and a renormalization of $H\beta$ were done simultaneously with the equation:

$$\frac{I(\lambda)}{I(H\beta)} = \frac{F(\lambda)}{F(H\beta)} 10^{f(\lambda)C(H\beta)} \left(1 - \frac{EW_{abs}(\lambda)}{EW(\lambda)} \right) \times \left(1 - \frac{EW_{abs}(H\beta)}{EW(H\beta)} \right)^{-1} \frac{100}{\eta}, \quad (1)$$

where $C(H\beta)$ is the reddening coefficient, $F(\lambda)$ is the absolute flux for each line, $EW(\lambda)$ is the equivalent width observed in λ and $EW_{abs}(\lambda) = EW_{abs}(H\beta) \times g(\lambda)$ is the theoretical equivalent width (Peña-Guerrero et al. 2012). Only the H and He lines were corrected for underlying absorption. This underlying absorption is due to the contribution of dust scattered light, this contribution is expected to include in absorption the H and He lines present in the brightest stars.

Finally we used a χ^2 minimization routine to obtain the parameters $C(H\beta)$, $EW_{abs}(H\beta)$, and η , the fitted values for Region I were 0.159, 1.647, and 99.53, respectively. The values for our best spectrum are in good agreement with the ones derived from Peimbert et al. (2012). Note that $H\beta$ is not normalized to 100 since with this value, the other lines of H, would be overestimated. In the same way that we want to average the helium lines, we want to do it with the hydrogen lines. We used the following Balmer lines $H\alpha$, $H\beta$, $H\gamma$, $H\delta$, $H11$, $H12$, and $H13$ to calculate the observations, this calculation implies that $H\beta = 99.53$. We decided to normalize the reddening-corrected fluxes using the 7 brightest Balmer lines. The best fit to these 7 lines yielded an $H\beta$ different than 100. We took the unconventional decision of choosing this $H\beta$ value, to avoid having to correct for the optimum value of H at a later stage.

Table 2 shows in columns (1) and (2) the adopted laboratory wavelength λ , and the identification for each line respectively,

the extinction law value used for each line (Seaton 1979) is in column (3), in columns (4) and (5) we present the flux $F(\lambda)$ and the intensity $I(\lambda)$ for each line (normalized to $H\beta$), and finally we show the % error for the intensity in column (6).

Table 2 List of emission line intensities.

λ	ID	$f(\lambda)$	$F(\lambda)^a$	$I(\lambda)^b$	% Error
3614	He I	0.282	0.64	0.70	6
3634	He I	0.280	1.08	1.18	4
3674	H I	0.269	0.40	0.48	8
3679	H I	0.268	0.27	0.35	10
3683	H I	0.267	0.35	0.45	8
3687	H I	0.266	0.39	0.52	8
3692	H I	0.265	0.55	0.72	8
3697	H I	0.264	1.02	1.26	6
3704	H I+He I	0.262	1.47	1.79	4
3712	H I	0.260	1.27	1.61	4
3722	H I	0.258	2.13	2.32	4
3726	[O II]	0.256	30.37	33.00	2
3729	[O II]	0.255	43.88	47.65	2
3734	H I	0.253	2.18	2.36	3
3750	H I	0.250	2.54	3.14	3
3771	H I	0.245	3.33	4.09	3
3789	C III?	0.240	0.12	0.13	15
3798	H I+[S III]	0.238	4.14	5.09	3
3820	He I	0.233	0.86	1.03	6
3829	Mn II?	0.231	0.50	0.53	8
3835	H I	0.229	6.31	7.53	2
3869	[Ne III]	0.222	35.95	38.58	1
3889	He I+H I	0.218	17.56	18.82	1.2
3970	H I	0.200	25.71	27.35	1
4009	He I + [Fe III]	0.194	0.59	0.63	6
4026	He I	0.190	1.79	2.07	4
4069	[S II]	0.182	1.00	1.06	6
4076	[S II]	0.181	0.55	0.59	8
4102	H I	0.176	24.62	27.00	1
4121	He I	0.173	0.20	0.30	12
4133	O II	0.171	0.11	0.11	15
4144	He I	0.169	0.16	0.27	12
4316	O II	0.135	0.38	0.39	8
4340	H I	0.128	45.95	48.47	1
4363	[O III]	0.122	6.82	7.06	2
4376	Ar II	0.119	0.14	0.15	15
4388	He I	0.116	0.48	0.56	8
4438	He I	0.100	0.23	0.24	10
4472	He I	0.094	3.80	4.03	3
4483	S II?	0.092	0.05	0.05	20
4529	Ne I	0.076	0.07	0.07	20
4563	...	0.070	0.09	0.10	15
4607	[Fe III]	0.055	0.05	0.05	20
4639+42	O II	0.051	0.06	0.06	20
4649+51	O II	0.049	0.12	0.12	15
4658	[Fe III]	0.047	0.30	0.30	10
4686	He II	0.041	0.24	0.24	10
4712	[Ar IV]+He I	0.034	1.10	1.10	6
4740	[Ar IV]	0.028	0.42	0.42	8
4769	[Fe III]	0.023	0.07	0.07	20
4861	H I	0.000	100.00	*99.53	0.8
4881	[Fe III]	-0.004	0.16	0.16	12
4922	He I	-0.013	1.08	1.13	6
4959	[O III]	-0.021	178.21	175.16	0.8
4986	[Fe III]	-0.027	0.29	0.29	10
5007	[O III]	-0.032	534.12	522.70	0.8
5016	He I	-0.034	2.48	2.51	3
5048	He I	-0.041	0.13	0.21	12
5192	[Ar III]+[N I]	-0.073	2.04	1.97	4
5270	[Fe III]	-0.089	0.11	0.11	15
5326	Ne I	-0.096	0.26	0.25	10
5433	[Fe II]	-0.128	0.08	0.08	20
5518	[Cl III]	-0.140	0.41	0.38	8
5538	[Cl III]	-0.144	0.42	0.39	8
5755	[N II]	-0.192	0.08	0.07	20
5876	He I	-0.216	11.69	10.85	1.5
6312	[S III]	-0.286	1.78	1.61	4

Table 2 cont.

λ	ID	$f(\lambda)$	$F(\lambda)^a$	$I(\lambda)^b$	% Error
6548	[N II]	-0.320	2.18	1.95	4
6563	H I	-0.322	314.61	282.24	0.8
6583	[N II]	-0.324	4.28	3.83	3
6678	He I	-0.337	3.39	3.05	3
6716	[S II]	-0.342	8.32	7.40	1.5
6731	[S II]	-0.343	5.98	5.31	2
7065	He I	-0.383	2.40	2.13	3
7136	[Ar III]	-0.391	8.39	7.33	2
7281	He I	-0.406	2.27	1.99	3
7320	[O II]	-0.410	1.30	1.13	4
7330	[O II]	-0.411	1.07	0.93	6

^a $F(\lambda)$ in units of $F(H\beta) = 100.0$; $F(H\beta) = 1.57 \times 10^{-12}$ erg $\text{cm}^{-2}\text{s}^{-1}$.

^b $I(\lambda)$ in units of $I(H\beta) = 99.53$; $I(H\beta) = 2.26 \times 10^{-12}$ erg $\text{cm}^{-2}\text{s}^{-1}$.

* Note that $I(H\beta) = 99.53$, see text.

To determine the [O II] $\lambda\lambda 3726, 3729$ intensity we subtracted the contribution of the H13 and H14 Balmer lines, we also subtracted the contribution of the [S III] $\lambda 3722$ line that originates in the same upper level than [S III] $\lambda 6312$. Similarly the contribution of [Ar IV] to $I(4711)$ was obtained by subtracting the intensity of He I $\lambda 4713$. Finally the contribution of He I to $I(3889)$ was obtained after subtracting the expected contribution of H8 (based on the work by Storey & Hummer 1995).

4. PHYSICAL CONDITIONS

4.1. Temperatures and Densities from CELs

We calculated physical conditions through CELs, fitting the line ratios using PyNeb (Luridiana et al. 2015). Electron temperatures were determined using the [O III] $\lambda 4363/(\lambda 4959 + \lambda 5007)$, [O II] $(\lambda 7320 + \lambda 7330)/(\lambda 3726 + \lambda 3729)$, and [N II] $\lambda 5755/\lambda 6584$ auroral to nebular intensity ratios. Electronic densities were determined from the [O II] $\lambda 3726/\lambda 3729$, and [S II] $\lambda 6731/\lambda 6716$ ratios which are strongly density dependent.

In addition, we obtained the [Fe III] density from the computations by Keenan et al. (2001), using the $I(\lambda 4986)/I(\lambda 4658)$ ratio. This ratio is strongly dependent on density, going from $I(4986)/I(4658) \approx 1.0$ at $n_e = 100 \text{ cm}^{-3}$ to $I(4986)/I(4658) \approx 0.05$ at $n_e = 3000 \text{ cm}^{-3}$. This ratio is a good density indicator, particularly for low densities, since it is more density dependent than the [Cl III] and [Ar IV] determinations; moreover the Fe^{++} density is much more representative of the whole object than the O^+ and S^+ densities, since $\text{Fe}^{++}/\text{Fe} \approx 60\%$ while $\text{O}^+/\text{O} \approx 20\%$ and $\text{S}^+/\text{S} \approx 15\%$. The temperatures and densities are presented in Table 3.

Table 3
Temperature and density from CELs.

Temperature (K)	[OIII]	[OII]	[NII]
NGC 346	12871 \pm 98	12445 \pm 464	10882 \pm 767
Density (cm^{-3})	[OII]	[SII]	[FeIII]
NGC 346	23.7 \pm 8.2	32 \pm 21	101 \pm 17

4.2. Temperatures and Densities from RLs

We used the program Heliol4, which is an extension of the maximum likelihood method presented by Peimbert et al. (2000) to obtain values for the temperature and density from He I lines. Heliol4 code determines the He^+/H^+

ionic abundance, $n_e(\text{He I})$, $T_e(\text{He I})$, the optical depth of the line He I $\lambda 3889$, and $t^2(\text{He I})$ through the information on the line intensities of He I, and the information of the [O II] ($\lambda 7320 + \lambda 7330$)/($\lambda 3726 + \lambda 3729$) and the [O III] $\lambda 4363$ /($\lambda 4959 + \lambda 5007$) line ratios. For a full description of the method see Peimbert et al. (2007).

By using ten He I lines: $\lambda 3819$, $\lambda 3889$, $\lambda 4026$, $\lambda 4388$, $\lambda 4471$, $\lambda 4922$, $\lambda 5016$, $\lambda 5876$, $\lambda 6678$, and $\lambda 7065$, we obtained a temperature $T_e(\text{He I}) = 11400 \pm 550$ K, and a density $n_e(\text{He I}) < 10 \text{ cm}^{-3}$.

4.3. Temperature Inhomogeneities

To derive the ionic abundance ratios, the average temperature, and the temperature standard deviation, we use the formalism of t^2 (Peimbert 1967). This formalism takes into account the temperature structure inside the H II region.

Each ionic species, X^{i+} , has a unique value of average temperature and of thermal inhomogeneity given by:

$$T_0(X^{i+}) = \frac{\int T_e n_e n(X^{i+}) dV}{\int n_e n(X^{i+}) dV} \quad (2)$$

and

$$t^2(X^{i+}) = \frac{\int [T_e - T_0(X^{i+})]^2 n_e n(X^{i+}) dV}{T_0(X^{i+})^2 \int n_e n(X^{i+}) dV}, \quad (3)$$

where n_e and $n(X^{i+})$ are the electron and ion densities respectively, and V is the observed volume.

In general, RLs, emissivities are stronger when T_e is lower while, CELs, emissivities are stronger when T_e is higher; and, also in general, RL temperatures are lower than T_0 while CEL temperatures are higher than T_0 . Overall, each temperature has a different t^2 dependence; for instance the [O III] $4363/5007$ temperature, in the presence of thermal inhomogeneities, can be expressed as a function of T_0 and t^2 as:

$$T_{4363/5007} = T_0 \left[1 + \frac{t^2}{2} \left(\frac{91300}{T_0} - 3 \right) \right]; \quad (4)$$

equivalent equations can be derived for the [N II], [O II], and [S II] temperatures as well as for He I and Balmer continuum temperatures.

Since temperatures can be presented as a function of t^2 and T_0 , when one measures 2 different temperatures in principle one can obtain T_0 and t^2 . In practice one prefers one temperature that weighs preferably the hot regions (e.g. $T[\text{O III}]$), and one that weighs preferentially the cold regions (e.g. $T(\text{He I})$ or $T(\text{Bac})$).

Combining results from CELs and values from He I and using the `Helio14` code we found that the maximum likelihood values are: $t^2(\text{He}^+) = 0.033 \pm 0.017$ and $T_0 = 11900 \pm 450$ K. These values can be used to determine abundances in the high-temperature regions, due to the similar ionization potentials of He^+ and O^{++} . Determinations for t^2 values from observations of H II regions range between 0.020 and 0.120 (Peimbert et al. 2012). The t^2 value depends on the specific characteristics of the thermal structure of each nebula (or even of each fraction of nebula).

5. IONIC CHEMICAL ABUNDANCES

5.1. Heavy element ionic abundances

We have followed the t^2 formalism for chemical abundances as presented by Peimbert & Costero (1969). The first

step to do so is to derive the abundances using the so called direct method and then to correct for the presence of thermal inhomogeneities.

We have used a two-zone direct method characterized by the zones where low- and high-ionization ions are present: $T(\text{low})$ and $T(\text{high})$. $T(\text{low})$ is the mean of $T_e[\text{N II}]$, $T_e[\text{O II}]$ and $T_e[\text{S II}]$, while $T(\text{high})$ is $T_e[\text{O III}]$; we used $T(\text{low})$ for singly ionized heavy elements, and $T(\text{high})$ for multiple ionized elements.

We used `PyNeb` to made the computations (Luridiana et al. 2015). In Table 4 we present two values for each ionic abundance, the first value is obtained directly from `PyNeb` ($t^2 = 0.00$), and the second value is using the formalism of t^2 .

To obtain the ionic abundance using $t^2 \neq 0.00$, we used the equations by Peimbert et al. (2004):

$$\left[\frac{n_{\text{cel}}(X^{i+})}{n(\text{H}^+)} \right]_{t^2 \neq 0.00} = \frac{T(\text{H}\beta)^\alpha T(\lambda_{nm})^{0.5}}{T_{(4363/5007)}^{\alpha+0.5}} \times \exp \left[-\frac{\Delta E_n}{kT_{(4363/5007)}} + \frac{\Delta E_n}{kT(\lambda_{nm})} \right] \times \left[\frac{n_{\text{cel}}(X^{i+})}{n(\text{H}^+)} \right]_{t^2=0.00}, \quad (5)$$

where $\alpha = -0.89$ is the temperature dependence of $\text{H}\beta$, ΔE_n is the difference of energy between the ground and the excited level of the CEL, and $T(\lambda_{nm})$ and $T(\text{H}\beta)$ are line temperatures, as described by Peimbert (1967) (and represent the average emissivity of each line for the temperature distribution on the observed object) and can be written as:

$$T(\lambda_{nm}) = T_0 \left\{ 1 + \frac{t^2}{2} \left[\frac{(\Delta E_n/kT_0)^2 - 3\Delta E_n/kT_0 + 3/4}{\Delta E_n/kT_0 - 1/2} \right] \right\}, \quad (6)$$

and

$$T(\text{H}\beta) = T_0 \left[1 - \frac{t^2}{2} (1 - \alpha) \right]. \quad (7)$$

Table 4
Ionic abundances from collisional excitation lines for NGC 346.

Ion	$t^2 = 0.000$	$t^2 = 0.033 \pm 0.017$
N ⁺	5.87±0.02	5.97±0.06
O ⁺	7.41±0.05	7.54±0.08
O ⁺⁺	7.93±0.01	8.04±0.06
Ne ⁺⁺	7.22±0.01	7.33±0.06
S ⁺	5.55±0.03	5.65±0.06
S ⁺⁺	6.18±0.02	6.24±0.04
Ar ⁺⁺	5.54±0.01	5.60±0.03
Ar ⁺³	5.11±0.02	5.22±0.06
Cl ⁺⁺	4.37±0.03	4.47±0.06

In units of $12 + \log n(X^{i+})/n(\text{H})$.

5.2. Helium Abundance

To determine the He abundance we also used the 10 lines mentioned in Sec. 4.2 as input for the `Helio14` code. This code uses the effective recombination coefficients given by Storey & Hummer (1995) for H^+ and for the case of He^+ those given by Benjamin et al. (2002) and Porter et al. (2013). The collisional contribution was estimated from Sawey & Berrington (1993) and Kingdon & Ferland (1995), and we used the

calculations made by Benjamin et al. (2002) for the optical depth effects in the triplets.

The correction of the underlying stellar absorption is important for He I lines, therefore we used the values from González Delgado et al. (1999) to correct lines with $\lambda < 5000\text{\AA}$, and for lines redder than 5876\AA , we used the values of Peimbert et al. (2005). The ionic abundance of He^{++} was obtained from the $\lambda 4686$ line presented in Table 2, and the recombination coefficients given by Storey & Hummer (1995).

Table 5
Ionic abundances from recombination lines for NGC 346.

Ion	$t^2 = 0.000$	$t^2 = 0.033 \pm 0.017$
He^+	10.917 ± 0.004	10.915 ± 0.004
He^{++}	8.30 ± 0.04	8.30 ± 0.04

In units of $12 + \log n(X^i)/n(\text{H})$.

6. TOTAL ABUNDANCES

For most elements we cannot observe all their ionic stages; so, in general, ionization correction factors (ICFs) are required. The functional forms of those ICFs frequently depend on the depth, quality, and coverage of the spectra.

In general, for helium:

$$\begin{aligned} \frac{N(\text{He})}{N(\text{H})} &= \frac{N(\text{He}^0) + N(\text{He}^+) + N(\text{He}^{++})}{N(\text{H}^0) + N(\text{H}^+)} \\ &= \text{ICF}(\text{He}^0) \frac{N(\text{He}^+) + N(\text{He}^{++})}{N(\text{H}^+)}, \end{aligned} \quad (8)$$

for objects of low, and medium, degree of ionization, the presence of neutral helium within the H II region is important and the $\text{ICF}(\text{He}^0) > 1$; for H II regions with a high degree of ionization, as is NGC 346, we can consider that the presence of neutral helium within the nebula is negligible; however one must be careful as for objects with very high degree of ionization the $\text{ICF}(\text{He}^0) < 1.00$ (even if the correction for helium is always $\text{ICF}(\text{He}^0) \gtrsim 0.99$, when we are looking for a precise determination of Y_p , one should try to avoid such objects).

To determine an accurate He/H ratio a precise value of the $\text{ICF}(\text{He}^0)$ is needed. Previous computations by Luridiana et al. (2003); Peimbert et al. (2002, 2007); Relaño et al. (2002) showed that the $\text{ICF}(\text{He}^0) = 1.00$ for NGC 346, because there is no transition zone from ionized to neutral He and H regions. We note that their results were calculated using tailor-made photoionization models with the code CLOUDY (Ferland et al. 2013).

For oxygen, to obtain the total abundance, we considered that:

$$\frac{N(\text{O}^{3+})}{N(\text{O})} = \frac{N(\text{He}^{++})}{N(\text{He})}, \quad (9)$$

and

$$\text{ICF}(\text{O}^+ + \text{O}^{++}) = \frac{N(\text{O}^+) + N(\text{O}^{++}) + N(\text{O}^{3+})}{N(\text{O}^+) + N(\text{O}^{++})}; \quad (10)$$

therefore:

$$\frac{N(\text{O})}{N(\text{H})} = \text{ICF}(\text{O}^+ + \text{O}^{++}) \left[\frac{N(\text{O}^+) + N(\text{O}^{++})}{N(\text{H}^+)} \right], \quad (11)$$

where

$$\text{ICF}(\text{O}^+ + \text{O}^{++}) = \left[1 - \frac{N(\text{He}^{++})}{N(\text{He})} \right]^{-1}. \quad (12)$$

For nitrogen, and neon we obtained the total abundances using the ICFs by Peimbert & Costero (1969).

$$\frac{N(\text{N})}{N(\text{H})} = \text{ICF}(\text{N}^+) \left[\frac{N(\text{N}^+)}{N(\text{H}^+)} \right], \quad (13)$$

where

$$\text{ICF}(\text{N}^+) = \frac{N(\text{O}^+) + N(\text{O}^{++}) + N(\text{O}^{+3})}{N(\text{O}^+)}, \quad (14)$$

and

$$\frac{N(\text{Ne})}{N(\text{H})} = \text{ICF}(\text{Ne}^{++}) \left[\frac{N(\text{Ne}^{++})}{N(\text{H}^+)} \right], \quad (15)$$

where

$$\text{ICF}(\text{Ne}^{++}) = \frac{N(\text{O}^+) + N(\text{O}^{++}) + N(\text{O}^{+3})}{N(\text{O}^{++})}. \quad (16)$$

We observed the auroral lines of [S II] and [S III]. To obtain the total sulphur abundance we used the ICF proposed by Stasińska (1978):

$$\frac{N(\text{S})}{N(\text{H})} = \text{ICF}(\text{S}^+ + \text{S}^{++}) \left[\frac{N(\text{S}^+) + N(\text{S}^{++})}{N(\text{H}^+)} \right] \quad (17)$$

where

$$\text{ICF}(\text{S}^+ + \text{S}^{++}) = \left[1 - \left(1 - \frac{N(\text{O}^+)}{N(\text{O})} \right)^3 \right]^{1/3}. \quad (18)$$

For the case of argon, we have measurements for lines of [Ar III] and [Ar IV]; we used the calculations by Pérez-Montero et al. (2007):

$$\frac{N(\text{Ar})}{N(\text{H})} = \text{ICF}(\text{Ar}^{++} + \text{Ar}^{3+}) \left[\frac{N(\text{Ar}^{++}) + N(\text{Ar}^{3+})}{N(\text{H}^+)} \right] \quad (19)$$

where

$$\text{ICF}(\text{Ar}^{++} + \text{Ar}^{3+}) = 0.928 + 0.364(1-x) + \frac{0.006}{1-x}. \quad (20)$$

For chlorine, we have measurements for lines of [Cl III], and to obtain the total abundance we used a reimplementation of the ICF proposed by Delgado-Inglada et al. (2014):

$$\frac{N(\text{Cl})}{N(\text{H})} = \text{ICF}(\text{Cl}^{++}) \frac{N(\text{O}^+) + N(\text{O}^{++})}{N(\text{H}^+)} \frac{N(\text{Cl}^{++})}{N(\text{O}^+)}, \quad (21)$$

where

$$\text{ICF}(\text{Cl}^{++}) = 2.914 \left(1 - \left[\frac{N(\text{O}^{++})}{N(\text{O}^+) + N(\text{O}^{++})} \right]^{0.21} \right)^{0.75}. \quad (22)$$

In Table 6 we present the results for $t^2 = 0.00$ as well as for $t^2 = 0.033 \pm 0.017$.

6.1. X, Y, and Z values for NGC 346

To calculate the fraction of He by mass, we need to know the fraction of the heavy elements by mass. For low metallicity objects, like NGC 346, the O/Z ratio is expected to be $O/Z \approx 0.55$ (Peimbert et al. 2007); this ratio is slightly larger than for high metallicity objects where $O/Z \sim 0.40$, mainly due to the increase of the C/O ratio (Carigi & Peimbert 2011). Using $O/Z = 0.55$ thus we can estimate the full value of $Z = 0.0030$ and from that $Y = 0.2490$.

Table 6
Total abundances for NGC 346.

Element	$t^2 = 0.000$	$t^2 = 0.033 \pm 0.017$
He	10.918±0.004	10.916±0.004
N	6.50±0.03	6.61±0.07
O	8.05±0.02	8.19±0.08
Ne	7.33±0.02	7.48±0.08
S	6.40±0.03	6.44±0.08
Ar	5.70±0.02	5.82±0.07
Cl	5.37±0.04	5.47±0.07

In units of $12 + \log n(X)/n(H)$.

One of the most subtle effects that we need to include in the determination of primordial helium or helium in very hot objects, is the correction due to the collisional excitation of the Balmer lines. Since models in Peimbert et al. (2002) that were later used in Peimbert et al. (2007, 2016), we know that for NGC 346 to include this effect produces an increase of 0.0015 ± 0.0005 , consequently $X = 0.7465$, $Y = 0.2505$ and $Z = 0.0030$. In this work, the contribution by collisions to the intensity of He and H lines is considerably smaller than objects with higher electron temperature like SBS 0335–052 or I Zw 18. To minimize this particular error it is important to study O/H poor objects but not extremely poor. Therefore, if we wish to further minimize this error, we must observe colder objects, with heavy elements abundances similar to those of NGC 346.

7. PRIMORDIAL HELIUM ABUNDANCE

To obtain the Y_p value, we need to compute the fraction of helium present in the interstellar medium produced by galactic chemical evolution. For this purpose it was assumed that:

$$Y_p = Y - O \frac{\Delta Y}{\Delta O}, \quad (23)$$

where Y and O are the helium and oxygen abundances by mass. We adopted the determination $\Delta Y/\Delta O = 3.3 \pm 0.7$ by Peimbert et al. (2016). To obtain this value, they used the observations of brighter objects from Peimbert et al. (2007) and chemical the evolution models for galaxies of low mass and metallicity by Carigi & Peimbert (2008) and Peimbert et al. (2010).

Most determinations are dominated by systematic errors rather than statistical errors. We can decrease the statistical errors increasing the number of objects used to determine Y_p . Nevertheless, the systematic ones will not decrease.

In Table 7, we present the error budget of our determination. The error is derived from the same 13 sources considered in Peimbert et al. (2007). The most important source of error is due to the difficulty to correct for the collisional excitation of the Balmer lines; in very hot objects, $T_e \geq 15000$, this excitation produces a non negligible increase in the Balmer line intensities relative to the case B recombination and, if ignored, introduces a bias in the reddening correction deduced from the Balmer decrement, both effects affecting the calibration of all the lines in the spectra by up to a few percent; however, since this effect has not been studied extensively the corrections that can be applied are uncertain at best, and thus such objects should be avoided. Another important source of error comes from the temperature structure; this arises because most Y determinations are based on a single homogeneous temperature, $T(4363/5007)$, however the $T_e(\text{He I})$ is systematically lower showing the presence of temperature variations that should be included in the Y_p determination. The error

Table 7
Error budget in the Y_p determination.

Problem	Error	*	This paper
$\Delta O(\Delta Y/\Delta O)$ correction	Systematic	± 0.0010	± 0.0012
Rec. coefficients of He I	Systematic	± 0.0010	± 0.0010
Temperature structure	Statistical	± 0.0010	± 0.0010
Reddening correction	Systematic	± 0.0007	± 0.0007
Collisional excitation of He I	Statistical	± 0.0007	± 0.0007
Underlying absorption in He I	Statistical	± 0.0007	± 0.0007
Underlying absorption in H I	Statistical	± 0.0005	± 0.0007
Optical depth of He I triplets	Statistical	± 0.0005	± 0.0007
Collisional excitation of H I	Systematic	± 0.0015	± 0.0005
Rec. coefficients of H I	Systematic	± 0.0005	± 0.0005
He I and H I line intensities	Statistical	± 0.0005	± 0.0005
He ionization correction factor	Statistical	± 0.0005	± 0.0003
Density structure	Statistical	± 0.0005	± 0.0003

*Peimbert et al. (2007).

of $O(\Delta Y/\Delta O)$ correction implies the extrapolation to zero heavy-element content; based on chemical evolution models of galaxies of different types, it is found that Y/O is practically constant for objects with $O < 4 \times 10^{-3}$. To estimate the error in the reddening correction, we made comparisons among four classic extinction laws and a recent one; these laws are labeled S79 (Seaton 1979), W58 (Whitford 1958), CCM89 (Cardelli et al. 1989), and B07 (Blagrave et al. 2007). The systematic effect of $ICF(\text{He})$, has to be tested with tailor-made photoionization models for low-metallicity H II regions. A discussion of the remaining (smaller) sources errors is presented in Peimbert et al. (2007).

When compared with errors of the sample of 2007 we can see that some systematic errors go down because we are using the best-known object to determine Y_p ; while a few of the statistical errors go up because we are using a single object with a notable increase in $\Delta Y/\Delta O$. One of the advantages of NCG 346 is that the correction due to the collisional excitation of the Balmer lines is smaller 0.0015 ± 0.0005 in comparison with 0.0144 ± 0.0038 for SBS 0335–052, and the 0.0056 ± 0.0015 for the sample by Peimbert et al. (2007, 2016). Overall the total error goes down, and the Y_p value amounts to 0.2451 ± 0.0026 .

We can also compare with previous determinations for Y_p determined using only NCG 346: $Y_p = 0.2345 \pm 0.0026$ by Peimbert et al. (2000), $Y_p = 0.2384 \pm 0.0025$ by Peimbert et al. (2002), $Y_p = 0.2453 \pm 0.0033$ by Peimbert et al. (2007), and $Y_p = 0.2433 \pm 0.0034$ by Peimbert et al. (2016). The difference when comparing the values of 2000 and 2002 with those from 2007 and onward comes from a better model of NGC346, newer atomic data and a better understanding of the quantity and magnitude of the sources of error (particularly, the effects of the collisional excitation of the Balmer lines were ignored in the first two determinations).

To summarize there are several advantages in observing a nearby H II region. The higher spatial resolution allows us to isolate the windows that are contaminated by the light of bright stars. This allows us to reduce the starlight emission and therefore to obtain a greater signal to noise in the emission lines. In this determination, the systematic errors due to collisional excitation of the H are smaller and some statistical errors (like the $ICF(\text{He}^0)$ and the density structure), also become smaller.

It is useful to discuss the determination of Y_p as a function time, Skillman et al. (2012) presents the plot with results from 1974 to 2012, accordingly in Figure 6 we present the Y_p results

from 2007 to the present. It is clear that the Y_p values derived by different groups provide an important constraint to the big bang theory. The main source of error is due to systematic uncertainties. In addition, the result by the Planck Collaboration et al. (2016), corresponds to $Y_p = 0.24467 \pm 0.0002$.

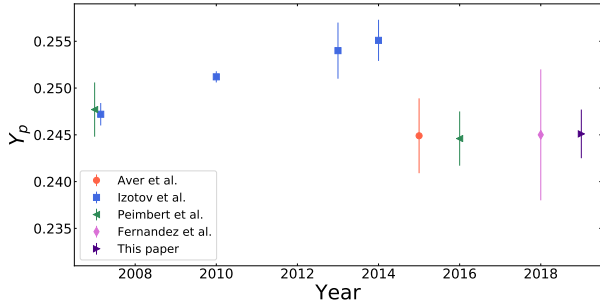


Figure 6. Measurements Y_p of the last 12 years, using H II regions.

8. DISCUSSION AND CONCLUSIONS

Low-metallicity H II regions are optimal objects to determine the primordial helium abundance. In this context, we studied the H II region NGC 346. By measuring its He I line intensities, we determined a primordial helium abundance $Y_p = 0.2451 \pm 0.0026$.

Table 8 shows Y_p measurements reported in the literature and in this work. Our Y_p value is consistent with most of the previous estimates. We note that the Izotov et al. (2014) determination differs significantly from the other values. We consider that they have some systematic errors that they are ignoring; for example, part of this difference is due to the adopted temperature structure: Izotov et al. (2014) used the temperature from CLOUDY photoionized models (Ferland et al. 2013), which predict $0.000 < t^2 < 0.015$, with a typical value of about 0.004 (Peimbert et al. 2017); alternatively the observed t^2 values for 28 H II regions are in the 0.019 to 0.120 range with an average value of 0.044 (Peimbert et al. 2012). A discussion on the possible reasons for the high t^2 values observed in H II regions is given by Peimbert et al. (2016).

Since the regions observed in all cases are not the same, we do not expect the values to be the same, e.g. there may be regions where the t^2 value may be higher due to stellar winds or other sources of energy input (e.g., Peimbert et al. 2017).

According to our error budget presented in Table 7 it is comforting that three of the other four independent Y_p results are very similar to ours. The main points of our result are: a) the lower temperature of NGC 346 reduces considerably the collisional excitation of the hydrogen lines as well as the uncertainty of its determination, when compared to the other samples, all of which include a few very hot objects, and b) the small error introduced by correcting for the underlying absorption of the He I lines in NGC 346, this is because we were able to eliminate most of the contribution of the dust scattered stellar light in our observations.

Peimbert et al. (2016) presents a Y_p value determined only using NGC 346; that determination has its error divided into statistical and systematical components that amounts 0.0028 and 0.0019 respectively, while in this paper the statistical error has been diminished to 0.0018 and the systematical one remains at 0.0019. The systematical error was not expected

to change, since we are using the same atomic data, the same reddening law, etc.; on the other hand the statistical error was indeed expected to diminish due to the greater quality of the data (the bigger telescope and the higher number of photons collected).

While this is a significant improvement over previous determinations, we would still like better determinations. To continue the quest to obtain a Y_p value of higher precision, we need: a) helium atomic data of higher quality; b) better chemical evolution models of dwarf galaxies, that would allow us to have a better determination of the $\Delta Y/\Delta O$ ratio; and c) a newer study of the reddening law, one designed to take full advantage of the newer telescopes and instruments that were not available a few decades ago. We also consider that observations, of objects like NCG 346, with the future generation extra-large telescopes will help reduce the error in the Y_p determination.

Table 8

Y_p values and predicted equivalent number of neutrino families, N_ν .

Y_p source	Y_p	N_ν
Izotov et al. (2014)	0.2551 ± 0.0022	3.58 ± 0.16
Aver et al. (2015)	0.2449 ± 0.0040	2.91 ± 0.30
Peimbert et al. (2016)	0.2446 ± 0.0029	2.89 ± 0.22
Fernández et al. (2018)	0.245 ± 0.007	2.92 ± 0.55
This work	0.2451 ± 0.0026	2.92 ± 0.20

Assuming $\tau_n = 880.2$ s (Tanabashi et al. 2018).

We estimated the number of neutrino families, N_ν , using the Y_p values reported in Table 8 assuming a neutron half-life value $\tau_n = 880.2 \pm 1.0$ s by Tanabashi et al. (2018). Table 8 shows the N_ν values from the previous cited authors. As expected the result in this paper is consistent with the results by Aver et al. (2015), Peimbert et al. (2016), and Fernández et al. (2018); these results agree with the presence of three families of neutrinos, which is consistent with laboratory determinations (e.g., Mangano et al. 2005; Mangano & Serpico 2011). While the Y_p result by Izotov et al. (2014) suggests the presence of a fourth neutrino family, which would not be fully ultrarelativistic (light) at the time of neutrino decoupling.

Table 9

Y_p values and the neutron mean life, τ_n .

Y_p source	Y_p	τ_n
Izotov et al. (2014)	0.2551 ± 0.0022	921 ± 11
Aver et al. (2015)	0.2449 ± 0.0040	872 ± 19
Peimbert et al. (2016)	0.2446 ± 0.0029	870 ± 14
Fernández et al. (2018)	0.245 ± 0.007	872 ± 33
This work	0.2451 ± 0.0026	873 ± 13

Assuming $N_\nu = 3.046$ (Mangano et al. 2005).

We also estimate the value of the neutron mean life, τ_n using the value of N_ν reported by Mangano et al. (2005), together with the Y_p estimations in Table 9. The results obtained from Aver et al. (2015), Peimbert et al. (2016), Fernández et al. (2018), and ourselves, are within 1σ from the value presented by Tanabashi et al. (2018), and they are in agreement with the τ_n laboratory determinations. Alternatively from the Y_p results obtained by Izotov et al. (2014), the τ_n value differs by more than 3σ from the laboratory determination.

We are grateful to the anonymous referee for a careful read-

ing of the manuscript and some excellent suggestions. We are indebted to Maria Teresa Ruiz for her collaboration in the observations of this object. We acknowledge CONACyT for supporting this project through grant 241732. M. V. acknowledges several constructive suggestions in Python by Oscar Barragán.

REFERENCES

Aver, E., Olive, K. A., & Skillman, E. D. 2015, *JCAP*, 7, 011
 Benjamin, R. A., Skillman, E. D., & Smits, D. P. 2002, *ApJ*, 569, 288
 Blagrove, K. P. M., Martin, P. G., Rubin, R. H., et al. 2007, *ApJ*, 655, 299
 Cardelli, J. A., Clayton, G. C., & Mathis, J. S. 1989, in *IAU Symposium*, Vol. 135, *Interstellar Dust*, ed. L. J. Allamandola & A. G. G. M. Tielens, 5
 Carigi, L., & Peimbert, M. 2008, *RMxAA*, 44, 341
 —, 2011, *Revista Mexicana de Astronomia y Astrofisica*, 47, 139
 Delgado-Inglada, G., Morisset, C., & Stasińska, G. 2014, *MNRAS*, 440, 536
 Ferland, G. J., Izotov, Y., Peimbert, A., et al. 2010, in *IAU Symposium*, Vol. 268, *Light Elements in the Universe*, ed. C. Charbonnel, M. Tosi, F. Primas, & C. Chiappini, 163
 Ferland, G. J., Porter, R. L., van Hoof, P. A. M., et al. 2013, *RMxAA*, 49, 137
 Fernández, V., Terlevich, E., Díaz, A. I., Terlevich, R., & Rosales-Ortega, F. F. 2018, *MNRAS*, 478, 5301
 González Delgado, R. M., Leitherer, C., & Heckman, T. M. 1999, *ApJS*, 125, 489
 Hamuy, M., Suntzeff, N. B., Heathcote, S. R., et al. 1994, *PASP*, 106, 566
 Hamuy, M., Walker, A. R., Suntzeff, N. B., et al. 1992, *PASP*, 104, 533
 Hilditch, R. W., Howarth, I. D., & Harries, T. J. 2005, *MNRAS*, 357, 304
 Izotov, Y. I., Thuan, T. X., & Guseva, N. G. 2014, *MNRAS*, 445, 778
 Keenan, F. P., Aller, L. H., Ryans, R. S. I., & Hyung, S. 2001, *Proceedings of the National Academy of Science*, 98, 9476
 Kingdon, J., & Ferland, G. J. 1995, *ApJ*, 442, 714
 Luridiana, V., Morisset, C., & Shaw, R. A. 2015, *A&A*, 573, A42
 Luridiana, V., Peimbert, A., Peimbert, M., & Cerviño, M. 2003, *ApJ*, 592, 846
 Mangano, G., Miele, G., Pastor, S., et al. 2005, *Nuclear Physics B*, 729, 221
 Mangano, G., & Serpico, P. D. 2011, *Physics Letters B*, 701, 296
 Massey, P., Parker, J. W., & Garmany, C. D. 1989, *AJ*, 98, 1305
 Mathis, J. S., & Rosa, M. R. 1991, *A&A*, 245, 625
 Pagel, B. E. J., Simonson, E. A., Terlevich, R. J., & Edmunds, M. G. 1992, *MNRAS*, 255, 325
 Peña-Guerrero, M. A., Peimbert, A., Peimbert, M., & Ruiz, M. T. 2012, *ApJ*, 746, 115
 Peimbert, A., Peña-Guerrero, M. A., & Peimbert, M. 2012, *ApJ*, 753, 39
 Peimbert, A., Peimbert, M., & Luridiana, V. 2002, *ApJ*, 565, 668
 —, 2016, *RMxAA*, 52, 419
 Peimbert, A., Peimbert, M., & Ruiz, M. T. 2005, *ApJ*, 634, 1056
 Peimbert, M. 1967, *ApJ*, 150, 825
 Peimbert, M., & Costero, R. 1969, *Boletín de los Observatorios Tonantzintla y Tacubaya*, 5, 3
 Peimbert, M., Luridiana, V., & Peimbert, A. 2007, *ApJ*, 666, 636
 Peimbert, M., Peimbert, A., Carigi, L., & Luridiana, V. 2010, in *IAU Symposium*, Vol. 268, *Light Elements in the Universe*, ed. C. Charbonnel, M. Tosi, F. Primas, & C. Chiappini, 91
 Peimbert, M., Peimbert, A., & Delgado-Inglada, G. 2017, *PASP*, 129, 082001
 Peimbert, M., Peimbert, A., & Ruiz, M. T. 2000, *ApJ*, 541, 688
 Peimbert, M., Peimbert, A., Ruiz, M. T., & Esteban, C. 2004, *ApJS*, 150, 431
 Peimbert, M., & Torres-Peimbert, S. 1974, *ApJ*, 193, 327
 Peimbert, M., Torres-Peimbert, S., & Ruiz, M. T. 1992, *RMxAA*, 24, 155
 Pérez-Montero, E., Hägele, G. F., Contini, T., & Díaz, A. I. 2007, *MNRAS*, 381, 125
 Planck Collaboration, Ade, P. A. R., Aghanim, N., et al. 2016, *A&A*, 594, A13
 Porter, R. L., Ferland, G. J., Storey, P. J., & Detisch, M. J. 2013, *MNRAS*, 433, L89
 Relaño, M., Peimbert, M., & Beckman, J. 2002, *ApJ*, 564, 704
 Sawey, P. M. J., & Berrington, K. A. 1993, *Atomic Data and Nuclear Data Tables*, 55, 81
 Seaton, M. J. 1979, *MNRAS*, 187, 73P
 Skillman, E., Aver, E., & Olive, K. 2012, *Memorie della Societa Astronomica Italiana Supplementi*, 22, 164
 Stasińska, G. 1978, *A&A*, 66, 257
 Storey, P. J., & Hummer, D. G. 1995, *MNRAS*, 272, 41
 Tanabashi, M., Hagiwara, K., Hikasa, K., et al. 2018, *Phys. Rev. D*, 98, 030001
 Viegas, S. M., Gruenwald, R., & Steigman, G. 2000, *ApJ*, 531, 813
 Vilchez, J. M. 1989, *Ap&SS*, 157, 9
 Whitford, A. E. 1958, *AJ*, 63, 201
 Zhang, Y., & Liu, X.-W. 2003, *A&A*, 404, 545